The electronic structure of 2(5H)-thiophenone investigated by vacuum ultraviolet synchrotron radiation and theoretical calculations

Sarvesh Kumar, Denis Duflot, Nikola C. Jones, Søren Vrønning Hoffmann, Gustavo García, Paulo Limão-Vieira

The electronic structure of 2(5H)-thiophenone investigated by vacuum ultraviolet synchrotron radiation and theoretical calculations*

S. Kumar[1,2], D. Duflot[3,4,a], N. C. Jones[5], S.V. Hoffmann[5], G. García[6], and P. Limão-Vieira[1,a]

[1] Atomic and Molecular Collisions Laboratory, CEFITEC, Department of Physics, Universidade NOVA de Lisboa, 2829-516 Caparica, Portugal

[2] Chemical Sciences Division, Lawrence Berkeley National Laboratory, One Cyclotron Road, Berkeley, 94720, California, USA

[3] UMR 8523 - Physique des Lasers Atomes et Molécules, Univ. Lille, F-59000 Lille, France

[4] CNRS, UMR 8523, F-59000 Lille, France

[5] ISA, Department of Physics and Astronomy, Aarhus University, Ny Munkegade 120, DK-8000, Aarhus C, Denmark

[6] Instituto de Física Fundamental, Consejo Superior de Investigaciones Científicas (CSIC), Serrano 113-bis, 28006 Madrid, Spain

Abstract

The absolute photoabsorption cross-sections for 2(5H)-thiophenone in the 3.7–10.7 eV energy range were measured using synchrotron radiation. New quantum chemical calculations performed at the equation of motion coupled cluster singles and doubles (EOM-CCSD) level were used to qualitatively interpret the photoabsorption spectrum. The electronic state spectroscopy of C_4H_4OS reveals the valence and Rydberg character of the lowest-lying excited states, with relevant C = O, C = C and C – C stretching vibrations across the entire absorption spectrum. Photolysis lifetimes in the Earth's atmosphere have been estimated from the absolute photoabsorption cross-sections, indicating that solar photolysis is expected to be a strong sink mechanism.

Keywords: 2(5H)-thiophenone, photoabsorption, VUV, cross-section, Rydberg states

Supplementary Information The online version contains supplementary material available at XXX

* We dedicate this contribution to the memory of the late Professor Michael Brunger with whom we have kept a fruitful and loyal scientific cooperation for almost two decades.

[a] e-mail: plimaovieira@fct.unl.pt (Paulo Limão-Vieira); denis.duflot@univ-lille.fr (Denis Duflot)

1 Introduction

In this contribution we continue investigating the electronic state spectroscopy of five-membered ring sulphur containing compounds and derivatives, with special attention to 2(5H)-thiophenone, C_4H_4OS. We have recently considered the lowest-lying valence, mixed valence-Rydberg and Rydberg states of thiophene (C_4H_4S) [1], due to its role in materials science and in the synthesis of conjugated π-systems, while the two isomeric chlorinated derivatives 2-chlorothiophene and 3-chlorothiophene, C_4H_3ClS [2], have encountered relevance as key selected elements for new optoelectronic materials [3,4]. The role of 2(5H)-thiophenone, C_4H_4OS, has been recognized relevant in biological and pharmaceutical applications (e.g., treatment of common heart and cancer diseases) [5] (and references therein), yet its main role has been closely related to the production of synthetic targets and intermediates [6].

Within the relevance of the current work, we note valence shell photoelectron studies on the lowest-lying ionic states [7] and Fourier transform infrared spectroscopy in low-temperature inert matrix [8]. Experiments on photoinduced ring-opening reaction with internal conversion and intersystem crossing [9] and with ultrafast transient infrared spectroscopy [10] have been reported. Additionally, 2(5H)-thiophenone has also been investigated by theoretical methods on the geometrical and electronic structure of the neutral molecule [9–12].

A thorough literature survey reveals no previous detailed information on the low-lying electronic states of C_4H_4OS in the 3.7–10.7 eV energy range, so we provide for the first time a comprehensive assessment of 2(5H)-thiophenone electronic state spectroscopy (the lowest-lying neutral and ionic states) by combining high-resolution vacuum ultraviolet (VUV) photoabsorption measurements with state-of-the art theoretical calculations at the equation of motion coupled cluster singles and doubles (EOM-CCSD) level of theory. The experimental absolute photoabsorption cross-section values are used for modelling such chemical compound in terrestrial atmosphere (see Section 4.5). In the next section we present a summary of the structure and properties of 2(5H)-thiophenone. A brief discussion of the experimental details and the computational methods employed in the calculations are given in Section 3. Section 4 is devoted to the results and discussion, and the absolute photoabsorption cross sections are used to calculate photolysis rates from 0–50 km altitude in the Earth's atmosphere. Finally, some conclusions that can be drawn from this study are given in Section 5.

2 Structure and properties of 2(5H)-thiophenone

The 2(5H)-thiophenone molecule, (C_4H_4OS), has C_S symmetry (A′ and A″) in its electronic ground-state with calculated valence electronic configuration of the $\tilde{X}\,{}^1A'$ state as:

… (10a')² (11a')² (12a')² (13a')² (14a')² (15a')² (16a')² (2a″)² (17a')² (18a')² (19a')² (3a″)² (20a′)² (21a′)² (4a″)² (5a″)², while the ordering of (4a") and (21a') are reversed in Chin et al. [7]. The character of the ground-state MOs (see Supplementary Material (SM)) shows that the highest occupied molecular orbital (HOMO), 5a", is the S 3p lone pair (n_S) out of the molecular plane, while (HOMO-1), 4a", is mainly π(C=C). The third highest occupied molecular orbital (HOMO-2), 21a', is the O 2p lone pair orbital (n_O) in the molecular plane with some σ(C–S) bonding character. The photoabsorption features (Figs. 1–5) have been mainly assigned to electronic excitations, due to promotion of an electron from those MOs to valence and Rydberg character orbitals (see Table 1 for the calculated dominant excitation energies and oscillator strengths).

The 2(5H)-thiophenone photoabsorption spectrum shows features assigned to vibronic transitions, where the fine structure has been assigned to the main fundamental vibrational modes available from the infrared absorption data [8]. Assignments were performed from the existing energies (and wavenumbers) in the ground electronic state to 0.213 eV (1713.9 cm^{-1}) for C_2=O_6 stretching, $\nu_4'(a')$, 0.200 eV (1615.4 cm^{-1}) for C_3=C_4 stretching, $\nu_5'(a')$ and 0.078 eV (629.8 cm^{-1}) for S_1–C_2 stretching/C_2=O_6 in-plane bending/C_5–S_1 stretching, $\nu_{14}'(a')$(see atoms numbering in Fig. 1); note that the vibrational modes numbering has been performed based on the decreasing energy from the data of Breda et al. [8]. The notation X_m^n, with *m* and *n* denoting the initial and final vibrational states for the assignments of the vibronic structure (*X*) is adopted. However, when the 0_0^0 transition is not discernible, we use the notation X^n instead.

The four lowest experimental vertical (v)/adiabatic (ad) ionisation energies, needed to calculate the quantum defects associated with transitions to Rydberg orbitals, are taken from the photoelectron work of Chin and co-workers [7] to be 9.63 eV $(5a'')^{-1}$, 10.58 eV $(4a'')^{-1}$, 9.76 eV $(21a')^{-1}$ and 12.25 eV $(20a')^{-1}$, respectively.

3 Methodology

3.1 Experimental arrangement

The experimental arrangement to obtain high-resolution VUV photoabsorption spectra of 2(5H)-thiophenone (Fig. 1), has been reported before [13,14]. Briefly, synchrotron radiation produced by the ASTRID2 storage ring, Aarhus University, Denmark, was delivered at the AU-UV beam line to perform the experiments. The monochromatized light with a resolution of better than 0.08 nm passes through an absorption gas cell that is filled with vapour of the

molecular compound under investigation. The transmission windows (MgF_2) used to enclose the absorption cell set the lower wavelength limit of detection (115 nm), and the transmitted UV light detected by a photomultiplier tube (PMT). A capacitance manometer (Chell CDG100D) was used to monitor the sample's absolute pressure in the absorption gas cell and to avoid any saturation effects in the data recorded, the absorption cross-sections were carefully measured using a pressure within the range 0.04–0.30 mbar which was appropriate for the local cross-section, to have attenuations of 50% or less. Absolute photoabsorption cross-section values, σ, in units of megabarn (1Mb ≡ 10^{-18} cm^2), were obtained using the Beer-Lambert attenuation law: $I_t = I_0 e^{(-N\sigma l)}$, where I_t is the light intensity transmitted through the gas sample, I_o is that through the evacuated cell, N the molecular number density of C_4H_4OS, and l the absorption path length (15.5 cm).

The synchrotron beam ring current was monitored throughout the collection of each spectrum, and background scans were recorded with the cell evacuated. Accurate cross-section values are obtained by recording the VUV spectrum in small (5 or 10 nm) sections, allowing an overlap of at least 10 points between the adjoining sections. To compensate for beam decay in the storage ring, ASTRID2 operates in a "top-up" mode allowing the light intensity to be kept quasi-constant. The small variations (~2–3%) of the incident flux are normalized to the beam current in the storage ring. This methodology allows us to determine the accuracy of the photoabsorption cross-sections to within ± 5%. The proposed assignments of the recorded absorption features are listed in Tables 2–5.

The liquid sample of 2(5H)-thiophenone was purchased from Sigma-Aldrich, with a stated purity of 98%. The sample was degassed through repeated freeze-pump-thaw cycles.

3.2 Theoretical methods

The quantum chemical calculations were performed in the optimized geometry of 2(5H)-thiphenone (Supplementary Information (SI) Fig. S1), at the CCSD level of calculation with the aug-cc-pVTZ basis set from Dunning [15,16] for H, C and O. For the S atom, the modified aug-cc-p(V+d)Z from Dunning et al. [15] was employed. For the description of Rydberg excited states, the basis set was augmented at the mass centre of the molecule by a set (6s6p4d) of diffuse orbitals, taken from [9,16]. The excited electronic states were obtained for the ground-state optimized molecular geometry, employing the EOM-CCSD method [17] and the aug-cc-pV(T+d)Z+R basis set (Tables 1 and S1), using the MOLPRO 2019.1 code [18,19]. The nature of each excitation was assessed by visual inspection of the natural orbitals for each transition and the average value $\langle r^2 \rangle$ of the electronic cloud. The calculated vertical excitation

energies of the lowest singlet states (S1–S7) at different levels of theory have also been obtained and compared to previous results too (see Table S2). Similarly, the calculated vertical ionisation energies (CCSD geometry with the aug-cc-pV(T+d)Z basis set) using several methods are compared with the available experimental values are shown in Table S3.

4 Results and discussion

The VUV photoabsorption spectrum of 2(5H)-thiophenone measured at room temperature is shown in Fig. 1 in the photon energy range 3.7–10.7 eV, while expanded views are shown in Figs. 2–5. To help interpreting the spectrum, our EOM-CCSD calculations are summarized in Table 1, while complete calculated vertical excitation energies are in Table S1, Supplementary Material. The spectroscopic assignments for the different bands are detailed in Tables 2–5 together with the calculated vertical excitation energies of the singlet states (S1–S7) and the lowest-lying ionic states (Tables S2 and S3). The major absorption bands can be classified as originating from valence and Rydberg excitations (see Section 4.4) converging to the lowest-lying ionic states, $(5a'')^{-1}\ \tilde{X}\,^2A''$, $(4a'')^{-1}\ \tilde{A}\,^2A''$, $(21a')^{-1}\ \tilde{B}\,^2A'$ and $(20a')^{-1}\ \tilde{C}\,^2A'$. Table 1 compares the EOM-CCSD results with the experimental data, where a reasonably good level of agreement is obtained (a few tenths of 1 eV). The different spectral sections exhibit fine structures, which have been assigned to C_2=O_6 stretching, C_3=C_4 stretching and S_1–C_2 stretching/C_2=O_6 in-plane bending/C_5–S_1 stretching modes, already dominant above 3.7 eV (Fig. 2). The broadness of the photoabsorption bands above 7.0 eV, albeit the fine structure superimposed on these, are mostly due to the overlap of different Rydberg electronic states. As a consequence of such contributions (vibronic excitations in valence and Rydberg states) the spectrum is quite congested and most of the assignments are not depicted on Figs. 2–5 but rather listed in Tables 2–5. The normal mode description of vibrations is relevant throughout the entire photoabsorption spectrum with special attention to the lowest-lying excitations, with the possibility of Fermi resonances.

The main electronic transitions of the photoabsorption bands are assigned to the promotion of an electron from the n_S (HOMO), π_{CC} (HOMO-1) and in-plane oxygen lone pair n_O (HOMO-2) to lowest unoccupied molecular orbitals (Tables 1 and S1, Fig. S2). The following sections present a detailed description of the photoabsorption features in the different photon energy ranges, together with the help of quantum chemical calculations.

4.1 Electronic excitation in the energy range 3.7 – 7.0 eV

Fig. 2a depicts a broad spectral feature with weak vibrational features that have been assigned in Table 2. The photoabsorption cross-section in this region peaks at 4.787 eV with a value of 5.94 Mb, and the calculations suggest this transition to be due to $\pi^*_{CC} + \pi^*_{CO}(6a'') \leftarrow n_S(5a''), \left(2\,{}^1A' \leftarrow \tilde{X}\,{}^1A'\right)$ with an oscillator strength of 0.05785 (Table 1). However, another less intense electronic transition at 4.028 eV, $f_L \approx 0.0004$, (Fig. 2b) is due to promotion of an electron from the HOMO-2 (21a′) to the LUMO (6a″), $\pi^*_{CC} + \pi^*_{CO}(6a'') \leftarrow n_O(21a'), \left(1\,{}^1A'' \leftarrow \tilde{X}\,{}^1A'\right)$. The rather low-intensity of the band is related to the poor overlap between the in-plane $n_O(21a')$and the out-of-plane LUMO (6a″). ~~A′ electronic ground-state excitation to the A″ state upper electronic state, which is polarised normal to the plane of the molecule.~~ Note that similar behaviour has been recently noted in formic acid lowest-lying absorption band [20]. The calculations in Table 1 reveal that the electronic transitions from the ground-state to $1\,{}^1A''$ and $2\,{}^1A'$ show antibonding π^*_{CO} and π^*_{CC} characters (Fig. S2). Another relevant aspect of the spectroscopy of such absorption band pertains to the photoinduced processes investigated at 257 nm (4.644 eV) [9,10]. These authors have reported prompt ring-opening (< 1 ps) from the characteristic antisymmetric ketene stretching mode, yet ~ 60% of the photoexcited molecules find their way back to the parent S_0 state vibrationally excited [10]. This seems to be in line with the experiment evidence of the present absorption band. Interesting to note that cuts along the $R_{C–S}$ ring opening coordinate, involving the ground and the first ^{1}A′ and ^{1}A″ states, strong vibrational coupling between the states can be promoted by normal modes of a″ symmetry, allowing the excited system to return to the ground-state [10]. Although from the assignments no a″ vibrational modes have been noted, we cannot discard the possibility of their relevance to the absorption band.

The 2(5H)-thiophenone absorption band in the photon energy range 3.7–4.5 eV shows extensive vibrational pattern, which is reminiscent of such characters. A careful inspection of Fig. 2b shows contributions of the C_2=O_6 stretching, $\nu'_4(a')$, C_3=C_4 stretching, $\nu'_5(a')$ S_1–C_2 stretching/C_2=O_6 in-plane bending/C_5–S_1 stretching, $\nu'_{14}(a')$ modes, with the average vibrational spacing being of 0.210, 0.190 and 0.072 eV, respectively (Table 2), although the origin of the band is not discernible. A detailed analysis of Fig. 2b also reveals a change in the slope of the band at ~ 4.1 eV. This can suggest the presence of another underlying state contributing to the spectrum. Xie et al. [9] calculated vertical excitation energies of the three lowest triplet states (T1–T3) at different levels of theory, with T1 at ~ 4.12 eV (95 kcal mol^{-1}). While such forbidden transition is indiscernible in experimental photoabsorption spectrum, the low intensity of the band (< 0.2 Mb) may be related in some way to a contribution of this nature.

The next electronic transition has its 0_0^0 origin at 5.75(6) eV (Table 3) and the maximum of the absorption band peaks at 6.344 eV with a cross-section of 23.21 Mb. The calculations in Table 1 assign the electronic transition to promotion of an electron from the HOMO-1 (4a″) to the LUMO (7a″), $\pi_{CC}^* + \pi_{CO}^*(6a'') \leftarrow \pi_{CC}(4a'')$, $\left(3\,^1A' \leftarrow \tilde{X}\,^1A'\right)$, with an oscillator strength of 0.14547. Although the major transitions predicted in the calculations for this energy region are valence in character, two Rydberg states are also tentatively assigned in Table 5, at 6.344 eV (4sσ ← 5a″) and 6.37(1) eV (4sσ ← 21a′), which will be discussed in Section 4.4. Nevertheless, analysis of 5.5–7.0 eV energy region shows that the C_2=O_6 stretching, $v_4'(a')$, C_3=C_4 stretching, $v_5'(a')$ and S_1–C_2 stretching/C_2=O_6 in-plane bending/C_5–S_1 stretching, $v_{14}'(a')$ modes are active, with the average vibrational spacing of 0.209, 0.183 and 0.065 eV, respectively (Table 3). On the higher energy side of the band (above 6.5 eV, see Fig. 3), at 6.93(0) eV a broad feature with a cross-section value of 14.73 Mb, is assigned to $\pi_{CC}^* + \pi_{CO}^*(22a') \leftarrow n_O(5a'')$, $\left(4\,^1A' \leftarrow \tilde{X}\,^1A'\right)$ transition (Table 1).

Table S2 shows the calculated vertical excitation energies at different levels of theory compared with previous work and the present experimental data. The level of agreement between the experimental data for S1 (4.028 eV) and S2 (4.787 eV) is very good with MS-CASPT2/cc-pVDZ [9] and ADC(2)/aug-cc-pV(T+d)Z+R, while S3 (6.344 eV) is better described by CASPT2/SA3-CAS(10,8)/6-31G*/MM [11]. Due to the closeness between the calculated S4 and S5 states, from the experiment we can only discern the latter (6.930 eV) which is reasonably obtained at the RS2C/SA-CAS(6,15)/aug-cc-pV(T+d)Z+R level of theory from multi-reference calculations. Table S2 emphasises the fact that the calculated lowest lying vertical transition energies are very method and basis set dependent.

4.2 Electronic excitation in the energy range 7.0 – 8.5 eV

The next electronic transition has its 0_0^0 origin at 7.315 eV, a maximum intensity of 52.46 Mb at 7.827 eV, is assigned to a transition from the electronic ground-state to Rydberg orbitals, $3d\sigma(a') \leftarrow n_O(21a') + 3d\pi(a'') \leftarrow n_S(5a'')$, $\left(9\,^1A' \leftarrow \tilde{X}\,^1A'\right)$, with a calculated electronic radial spatial extent (144) indicative of such character (Table 1). The transition is mainly accompanied by excitation of C_2=O_6 stretching, $v_4'(a')$ (spacing 0.244 eV) with a few quanta of C_3=C_4 stretching, $v_5'(a')$ (spacing 0.195 eV) and S_1–C_2 stretching/C_2=O_6 in-plane bending/C_5–S_1 stretching, $v_{14}'(a')$ (spacing 0.061 eV) modes. Other Rydberg state excitation at 7.827 eV is assigned to (4pσ ← 4a″), yet this is thoroughly discussed in Section 4.4. This absorption band is shown in detail in Fig. 4 with the assignments of the spectral features in

Table 3. The structural features observed above the transitions, are also broad and originate from the contribution of the mixing character with other Rydberg $(5a'')^{-1}$ and $(21a')^{-1}$ series, also displaying a significant vibrational structure which are discussed in more detail below (see also Table 4).

From the calculated vertical excitation energies in Table S2 for the singlet excited state S7, RS2C/SA-CAS(6,15)/aug-cc-pV(T+d)Z+R level of theory from multi-reference calculations gives a better agreement with the experiment (to within 0.2 eV) while EOM-CCSD/aug-cc-pV(T+d)Z+R (7.022 eV) and ADC(2)/aug-cc-pV(T+d)Z+R (7.064 eV) underestimate it by 10%.

4.3 Electronic excitation in the energy range 8.5 – 10.7 eV

This band of the photoabsorption spectrum is dominated by a large number of spectral features that are assigned to members of the different Rydberg transitions converging to the $(5a'')^{-1}$ $\tilde{X}\,^2A''$, $(4a'')^{-1}$ $\tilde{A}\,^2A''$, $(21a')^{-1}$ $\tilde{B}\,^2A'$ and $(20a')^{-1}$ $\tilde{C}\,^2A'$ ionic states of 2(5H)-thiophenone (discussed in detail below). The features are mainly due to the overlap of the many different Rydberg electronic states and the superposition of the different vibrational modes contributing to the absorption spectrum (Table 4), thus contributing to the broadening of the absorption features as well as to augment others which otherwise would not manifest as so intense (Fig. 5). The calculations in Table 1 (and Table S1) do not predict any valence excitations in this photon energy region, despite the background contribution to the absorption spectrum. Note that in this region, and specially above 9.5 eV, photoionisation to the $(5a'')^{-1}$, $(4a'')^{-1}$ and $(21a')^{-1}$ states may contribute to the spectrum and so reducing the observable features within this region.

4.4 Rydberg series

The photoabsorption spectrum of 2(5H)-thiophenone exhibits a relevant Rydberg character (Figs. 3–5) across the majority of the bands, with the experimental energies, tentative assignments and quantum defects in Table 5. Table S3 lists the calculated valence and outer valence vertical ionisation energies (*IE*s) for 2(5H)-thiophenone at the EOM-CCSD/aug-cc-pV(T+d)Z, together with other different levels of theory, and compares with the experimental photoelectron data [7]. A close inspection of those tabulated values reveals that all the theoretical methods agree reasonably well with each other to within 0.1–0.3 eV, even though P3+ seems to be the more accurate, while those provided by the Koopmans' theorem are larger, which is due to neglection of electron correlations and relaxation. The P3+ and EOMIP-CCSD

[21] results are very close to each other while the EOMIP-CC3 method [22] tends to overestimate by as much as 6% the experimental data. The geometry of the 2(5H)-thiophenone was kept at C_S symmetry, in the optimized ground state geometry, as indicated in Fig. S1.

The assignment of each absorption feature position in the 2(5H)-thiophenone spectrum has been tested with the Rydberg formula: $E_n = IE - \frac{R}{(n-\delta)^2}$, where *IE* is the ionisation energy, *n* is the principal quantum number of the Rydberg orbital of energy E_n, *R* is the Rydberg constant (13.61 eV), and δ is the quantum defect resulting from the penetration of the Rydberg orbital into the core. For sulphur: $1.9 < \delta < 2.0$ for *n*s, $1.4 < \delta < 1.8$ for *n*p, and $0.1 < \delta < 0.5$ for *n*d [23]. As far as the authors are aware, no previous Rydberg features have been reported in the literature.

The lowest-lying Rydberg transition is assigned to the $(4s\sigma \leftarrow (5a''))$ excitation, with the first member (*n* = 4) at 6.344 eV and having a quantum defect δ = 1.96 (Table 5). Note that the shape of the absorption band, where the 4sσ member is assigned, is mostly of a valence character rather than Rydberg (see Fig. 3). Other transitions to the higher-order Rydberg members up to *n* = 10, of the $ns\sigma$ series, are also reported, while the features at 8.14(6), 9.100, 9.253 and 9.350 eV (*n* = 5sσ, 7sσ, 8sσ and 9sσ) have also been assigned to other Rydberg members 3dσ′(21a′)$^{-1}$, 6pπ(21a′)$^{-1}$, 6dσ′(5a″)$^{-1}$/5pσ(4a″)$^{-1}$, and 7dσ(5a″)$^{-1}$, respectively. The rather high value of the quantum defects for the 9s and 10s members are attributed to the influence of the other closest-lying Rydberg states.

The first members of the two n*p* ($np\sigma \leftarrow 5a''$) and ($np\pi \leftarrow 5a''$) series are associated with absorption features at 6.93(0) and 7.54(2) eV (δ = 1.75 and 1.45, respectively) (Table 5). The relatively high values of the present quantum defects, with special attention to the lowest absorption features can be attributed to a mixed valence character of these transitions, as discussed in Section 4.2. The 6pσ and 7pπ features at 8.847 and 9.18(4) eV can also be assigned to 3dσ(4a″)$^{-1}$ and 5dσ′(21a′)$^{-1}$. Our assignments also report the presence of two n*d* ($nd\sigma \leftarrow 5a''$) and ($nd\sigma' \leftarrow 5a''$) series, with the n = 3 features at 7.90(2) and 8.06(7) eV (δ = 0.19 and 0.05) (Table 5). The features at 8.698 (4dσ) and 9.05(7) eV (5dσ) are also assigned to 5pπ(21a′)$^{-1}$ and 5sσ(4a″)$^{-1}$. Note also that transitions to higher members of the nd Rydberg series, up to *n* = 7, are also discernible. No attempt was made to assign the higher members of the Rydberg series (n > 7), due to their low intensity in the absorption spectrum.

The Rydberg series converging to the ionic electronic first excited state are listed in Table 5 and have been assigned to the $(ns\sigma, np\sigma, np\pi, nd\sigma, nd\sigma' \leftarrow 4a'')$ transitions. The first members of the $ns\sigma, np\sigma, np\pi, nd\sigma$ and $nd\sigma'$ series are associated with features at 7.50(0) eV

(δ = 1.89), 7.827 eV (δ = 1.78), 8.51(8) eV (δ = 1.43), 8.84(7) eV (δ = 0.20) and 8.98(4) eV (δ = 0.08) (Table 5). Absorption features at 7.51(0) and 9.96(3) eV can also contribute to 4pπ(21a′)$^{-1}$ and 5dσ(4a″)$^{-1}$.

The Rydberg series converging to the ionic electronic second excited state have been assigned to the $(ns\sigma, np\sigma, np\pi, nd\sigma, nd\sigma' \leftarrow 21a')$ transitions. The first members of the $ns\sigma, np\sigma, np\pi, nd\sigma$ and $nd\sigma'$ series are associated with features at 6.37(1) eV (δ = 2.00), 7.42(4) eV (δ = 1.59), 7.51(0) eV (δ = 1.54), 7.99(9) eV (δ = 0.22) and 8.14(6) eV (δ = 0.10) (Table 5). The feature at 9.54(8) eV assigned to n = 10sσ is also due to a Rydberg transition to 4pσ(20a′)$^{-1}$.

Finally, the Rydberg series converging to the ionic electronic third excited state have been assigned to the $(ns\sigma, np\sigma, np\pi, nd\sigma \leftarrow 20a')$ transitions. The first members of the $ns\sigma, np\sigma, np\pi$ and $nd\sigma$ series are associated with features at 8.89(1) eV (δ = 1.99), 9.45(8) eV (δ = 1.76), 10.19(6) eV (δ = 1.43) and 10.50(7) eV (δ = 0.21) (Table 5). Tentative assignments of these series have only been made up to n = 4, because higher members lie outside the photon energy range investigated.

Vibrational excitation involving some of the Rydberg series converging to the $(5a'')^{-1}$, $(4a'')^{-1}$, $(21a')^{-1}$ and $(20a')^{-1}$ states have been assigned in Tables 3 and 4, and not included in Fig. 5 to avoid congestion. The fine structure has been assigned to the C_2=O_6 stretching, $v_4'(a')$, the C_3=C_4 stretching, $v_5'(a')$ and the S_1–C_2 stretching/C_2=O_6 in-plane bending/C_5–S_1 stretching, $v_{14}'(a')$ modes. Combination bands of these modes have also been assigned.

4.5 Absolute photoabsorption cross sections and atmospheric photolysis

The absolute cross-section values listed in Table 1 are related to the most representative electronic transitions. A comprehensive literature survey reveals no previous studies to compare with the ultraviolet photoabsorption data in the wavelength region 116 – 330 nm (3.7–10.7 eV) covered in the present work. The combination of high-resolution VUV absolute photoabsorption cross-sections and solar actinic flux measurements [24], can be used to calculate photolysis rates of 2(5H)-thiophenone in the Earth's atmosphere, from sea-level up to 50 km (the limit of the stratopause). To obtain such information and thus the local lifetime of a given molecular compound emitted to the atmosphere and subject to the interaction of solar ultraviolet radiation [25], we use a well-established methodology with details being found from the work of Limão-Vieira and co-workers [26]. The quantum yield for dissociation is assumed to be unity due to lack of any information in the literature. Computed photolysis lifetimes of

less than 1 sunlit day were calculated at altitudes above ground level, thus indicating that 2(5H)-thiophenone can be efficiently broken up by UV absorption at those altitudes. We are not aware of any complete study of the gas-phase kinetics for 2(5H)-thiophenone reactions with •OH radicals or any other radical relevant within the Earth's atmosphere (e.g., Cl, NO_3 and O_3) to assess the role of such processes as the main sink mechanism.

5 Conclusions

We have reported for the first time a comprehensive study of the electronic state spectroscopy of 2(5H)-thiophenone in the 3.7–10.7 eV photon energy range. The absolute values of the present measured high-resolution cross sections have been assigned to valence and Rydberg transitions, with the aid of quantum chemical calculations, on the vertical excitation energies and oscillator strengths. The joint experimental and theoretical methodology has allowed the assignment of the fine structure in the spectrum which is due to the contributions of C_2=O_6 stretching, $v_4'(a')$, C_3=C_4 stretching, $v_5'(a')$, and S_1–C_2 stretching/C_2=O_6 in-plane bending/C_5–S_1 stretching, $v_{14}'(a')$ modes. The photolysis lifetimes of 2(5H)-thiophenone were also obtained for the Earth's atmosphere, from 0 km up to 50 km (the limit of the stratopause), indicating that solar photolysis is expected to be a strong sink if no other relevant gas-phase reactions with •OH and other radicals present in the Earth's atmosphere (e.g., Cl, NO_3) prevail.

Acknowledgments

SK acknowledges the Portuguese National Funding Agency (FCT) through PD/BD/142831/2018 and COVID/BD/152673/2022, and together with PLV the research grant CEFITEC (UIDB/00068/2020). This work was also supported by Radiation Biology and Biophysics Doctoral Training Programme (RaBBiT, PD/00193/2012); UCIBIO (UIDB/04378/2020). D.D. thanks the support from the CaPPA project (Chemical and Physical Properties of the Atmosphere) funded by the French National Research Agency (ANR) through the PIA (Programme d'Investissement d'Avenir) under Contract No. ANR-10-LABX-005; the Région Hauts de France and the Ministère de l'Enseignement Supérieur et de la Recherche (CPER ECRIN) and the European Fund for Regional Economic Development for their financial support. This work was performed using HPC resources from GENCI-TGCC (Grant No. 2022–A0110801859) and the Centre de Ressources Informatiques (CRI) of the Université de Lille. The authors wish to acknowledge the beam time at the ISA synchrotron, Aarhus University, Denmark. The research leading to this work has been supported by the project CALIPSOplus

under the Grant Agreement 730872 from the EU Framework Programme for Research and Innovation HORIZON 2020. GG acknowledges the Spanish Ministerio de Ciencia e Innovación (Project No. PID2019-104727RB-C21). This contribution is also based upon work from the COST Action CA18212-Molecular Dynamics in the GAS phase (MD-GAS), supported by COST (European Cooperation in Science and Technology).

Author contributions

S.K. and N.C.J. performed the experimental measurements. D.D. performed the quantum chemistry calculations. S.K., N.C.J., S.V.H. and P.L.V. analyzed the data. P.L.V. and G.G. conceptualized and supervised the project. P.L.V. and D.D. wrote the manuscript.

Declarations

Conflict of interest

The authors declare that they have no known competing financial interests or personal relationships that could have appeared to influence the work reported in this paper.

ORCID

S. Kumar: 0000-0002-1996-9925

D. Duflot: 0000-0002-8307-5344

N. C. Jones: 0000-0002-4081-6405

S. V. Hoffmann: 0000-0002-8018-5433

G. García: 0000-0003-4033-4518

P. Limão-Vieira: 0000-0003-2696-1152

References

[1] D.B. Jones, M. Mendes, P. Limão-Vieira, F.F. Silva, N.C. Jones, S. V. Hoffmann, M.J. Brunger, Electronic structure and VUV photoabsorption measurements of thiophene, J. Chem. Phys. 150 (2019) 064303. https://doi.org/10.1063/1.5089505.

[2] F.V.S. Oliveira, A.S. Barbosa, N.C. Jones, S. V. Hoffmann, P. Limão-Vieira, The electronic spectra of 2- chlorothiophene and 3-chlorothiophene in the vacuum ultraviolet photoabsorption energy region (3.9–10.8 eV), J. Quant. Spectrosc. Radiat. Transfer. 296 (2023) 108443.

[3] N.L. Campbell, W.L. Duffy, G.I. Thomas, J.H. Wild, S.M. Kelly, K. Bartle, M. O'Neill, V. Minter, R.P. Tuffin, Nematic 2,5-disubstituted thiophenes, J. Mater. Chem. 12 (2002) 2706–2721. https://doi.org/10.1039/b202073b.

[4] M. Romanini, P. Negrier, M. Barrio, D. Mondieig, P. Serra, M.J. Zuriaga, R. Macovez, J.L. Tamarit, Structure and Dynamics of the Crystalline Stable Phase of 2-Chlorothiophene, Cryst. Growth Des. 19 (2019) 6405–6413. https://doi.org/10.1021/acs.cgd.9b00871.

[5] J.D. Coyle, Photochemistry of Carboxyiic Acid Derivatives, Chem. Rev. 78 (1978) 97–123. https://doi.org/10.1021/cr60312a002.

[6] N.B. Carter, A.E. Nadany, J.B. Sweeney, Recent developments in the synthesis of furan-2(5H)-ones, J. Chem. Soc., Perkin Trans. 1 (2002) 2324–2342. https://doi.org/10.1039/b007664n.

[7] W.S. Chin, Z.P. Xu, C.Y. Mok, H.H. Huang, H. Mutoh, S. Masuda, He I and He II photoelectron spectra of thiophenones, J. Electron Spectrosc. Relat. Phenom. 88–91 (1998) 97–101. https://doi.org/10.1016/s0368-2048(97)00253-3.

[8] S. Breda, I. Reva, R. Fausto, Molecular structure and vibrational spectra of 2(5H)-furanone and 2(5H)-thiophenone isolated in low temperature inert matrix, J. Mol. Struct. 887 (2008) 75–86. https://doi.org/10.1016/j.molstruc.2008.02.034.

[9] B. Bin Xie, B.L. Liu, X.F. Tang, D. Tang, L. Shen, W.H. Fang, Nonadiabatic dynamics simulation of photoinduced ring-opening reaction of 2(5H)-thiophenone with internal conversion and intersystem crossing, Phys. Chem. Chem. Phys. 23 (2021) 9867–9877. https://doi.org/10.1039/d1cp00281c.

[10] D. Murdock, S.J. Harris, J. Luke, M.P. Grubb, A.J. Orr-Ewing, M.N.R. Ashfold, Transient UV pump-IR probe investigation of heterocyclic ring-opening dynamics in the solution phase: The role played by nσ* states in the photoinduced reactions of thiophenone and furanone, Phys. Chem. Chem. Phys. 16 (2014) 21271–21279. https://doi.org/10.1039/c4cp03653k.

[11] B. Bin Xie, W.H. Fang, Combined Quantum Trajectory Mean-Field and Molecular Mechanical (QTMF/MM) Nonadiabatic Dynamics Simulations on the Photoinduced Ring-Opening Reaction of 2(5H)-Thiophenone, ChemPhotoChem. 3 (2019) 897–906. https://doi.org/10.1002/cptc.201900076.

[12] G.M.J. Barca, C. Bertoni, L. Carrington, D. Datta, N. De Silva, J.E. Deustua, D.G. Fedorov, J.R. Gour, A.O. Gunina, E. Guidez, T. Harville, S. Irle, J. Ivanic, K. Kowalski, S.S. Leang, H. Li, W. Li, J.J. Lutz, I. Magoulas, J. Mato, V. Mironov, H. Nakata, B.Q. Pham, P. Piecuch, D. Poole, S.R. Pruitt, A.P. Rendell, L.B. Roskop, K. Ruedenberg, T. Sattasathuchana, M.W. Schmidt, J. Shen, L. Slipchenko, M. Sosonkina, V. Sundriyal, A. Tiwari, J.L. Galvez Vallejo, B. Westheimer, M. Włoch, P. Xu, F. Zahariev, M.S. Gordon, Recent developments in the general atomic and molecular electronic structure system, J. Chem. Phys. 152 (2020) 154102. https://doi.org/10.1063/5.0005188.

[13] S. Eden, P. Limão-Vieira, S. V. Hoffmann, N.J. Mason, VUV photoabsorption in CF3X (X = Cl, Br, I) fluoro-alkanes, Chem. Phys. 323 (2006) 313–333.

[14] M.H. Palmer, T. Ridley, S.V. Hoffmann, N.C. Jones, M. Coreno, M. De Simone, C. Grazioli, M. Biczysko, A. Baiardi, P. Limão-Vieira, Interpretation of the vacuum ultraviolet photoabsorption spectrum of iodobenzene by ab initio computations, J. Chem. Phys. 142 (2015) 134302.
[15] J. Dunning, K.A. Peterson, A.K. Wilson, Gaussian basis sets for use in correlated molecular calculations. X. The atoms aluminum through argon revisited, J. Chem. Phys. 114 (2001) 9244–9253. https://doi.org/10.1063/1.1367373.
[16] D. Duflot, S.V. Hoffmann, N.C. Jones, P. Limão-Vieira, Synchrotron radiation UV-VUV photoabsorption of gas phase molecules, in: A.S. Pereira, P. Tavares, P. Limão-Vieira (Eds.), Radiation in Bioanalysis: Spectroscopic Techniques and Theoretical Methods, Springer, 2019: pp. 43–81.
[17] C. Hampel, K.A. Peterson, H.J. Werner, A comparison of the efficiency and accuracy of the quadratic configuration interaction (QCISD), coupled cluster (CCSD), and Brueckner coupled cluster (BCCD) methods, Chem. Phys. Lett.. 190 (1992) 1–12. https://doi.org/10.1016/0009-2614(92)86093-W.
[18] H.J. Werner, P.J. Knowles, G. Knizia, F.R. Manby, M. Schütz, Molpro: A general-purpose quantum chemistry program package, WIREs Comput. Mol .Sci. 2 (2012) 242–253. https://doi.org/10.1002/wcms.82.
[19] H.-J. Werner, P.J. Knowles, G. Knizia, F.R. Manby, M. Schütz, P. Celani, W. Györffy, D. Kats, T. Korona, R. Lindh, A. Mitrushenkov, G. Rauhut, K.R. Shamasundar, T.B. Adler, R.D. Amos, S.J. Bennie, A. Bernhardsson, A. Berning, D.L. Cooper, M.J.O. Deegan, A.J. Dobbyn, F. Eckert, E. Goll, C. Hampel, A. Hesselmann, G. Hetzer, T. Hrenar, G. Jansen, C. Köppl, S.J.R. Lee, Y. Liu, A.W. Lloyd, Q. Ma, R.A. Mata, A.J. May, S.J. McNicholas, W. Meyer, T.F.M. III, M.E. Mura, A. Nicklass, D.P. O'Neill, P. Palmieri, D. Peng, K. Pflüger, R. Pitzer, M. Reiher, T. Shiozaki, H. Stoll, A.J. Stone, R. Tarroni, T. Thorsteinsson, M. Wang, M. Welborn, MOLPRO, version 2019.1, a package of ab initio programs, (2019).
[20] P.A.S. Randi, D.F. Pastega, M.H.F. Bettega, N.C. Jones, S. V. Hoffmann, S. Eden, A. Souza Barbosa, P. Limão-Vieira, Electronically excited states of formic acid investigated by theoretical and experimental methods, Spectrochim. Acta, Part A. 289 (2023) 122237. https://doi.org/10.1016/j.saa.2022.122237.
[21] J.F. Stanton, J. Gauss, Analytic energy derivatives for ionized states described by the equation-of-motion coupled cluster method, J. Chem. Phys. 101 (1994) 8938–8944. https://doi.org/10.1063/1.468022.
[22] J.F. Stanton, J. Gauss, A simple scheme for the direct calculation of ionization potentials with coupled-cluster theory that exploits established excitation energy methods, J. Chem. Phys. 111 (1999) 8785–8788. https://doi.org/10.1063/1.479673.
[23] M.B. Robin, Higher Excited States of Polyatomic Molecules, Volume III, Academic Press, 1985.
[24] Chemical Kinetics and Photochemical Data for Use in Stratospheric Modelling, Evaluation number 12, NASA, Jet Propulsion Laboratory, JPL, Publication 97-4, January 15, 1997.
[25] D. Duflot, S.V. Hoffmann, N.C. Jones, P. Limão-Vieira, Synchrotron Radiation UV-VUV Photoabsorption of Gas Phase Molecules, in: A.S. Pereira, P. Tavares, P. Limão-Vieira (Eds.), Radiation in Bioanalysis Spectroscopic, Techniques and Theoretical Methods, Springer, 2019: pp. 43–81.
[26] P. Limão-Vieira, S. Eden, P.A. Kendall, N.J. Mason, S. V. Hoffmann, VUV Photo-Absorption Cross-Section for CCl2F2, Chem. Phys. Lett. 364 (2002) 535–541.

Figure captions

Fig. 1 The VUV photoabsorption cross-section in the 3.7–10.7 eV photon energy range for 2(5H)-thiophenone. Inset shows the structure of the molecule.

Fig. 2 The VUV photoabsorption cross-section of 2(5H)-thiophenone in the: (a) 3.7–6.0 eV and (b) 3.7–4.5 eV photon energy ranges.

Fig. 3 The VUV photoabsorption cross-section in the 5.5–7.0 eV photon energy range for 2(5H)-thiophenone.

Fig. 4 The VUV photoabsorption cross-section in the 7.0–8.5 eV photon energy range for 2(5H)-thiophenone.

Fig. 5 The VUV photoabsorption cross-section in the 8.5–10.7 eV photon energy range for 2(5H)-thiophenone.

Table captions

Table 1 Calculated vertical excitation energies (EOM-CCSD/aug-cc-pV(T+d)Z+R basis set) and oscillator strengths (singlet states) of 2(5H)-thiophenone (C_4H_4OS), compared with results from the present experimental data (all energies in eV). For a complete table see Supplementary Material Table S1. See details in text.

Table 2 Proposed vibrational assignments of 2(5H)-thiophenone absorption band in the photon energy range 3.7−4.5 eV[a]. Energies in eV. See text for details

Table 3 Proposed vibrational assignments of 2(5H)-thiophenone absorption bands in the photon energy range 5.5−8.5 eV[a]. Energies in eV. See text for details.

Table 4 Proposed vibrational assignments of 2(5H)-thiophenone absorption bands in the photon energy range 8.2−10.7 eV[a]. Energies in eV. See text for details.

Table 5 Energy values (eV), quantum defects (δ) and assignments of the Rydberg series converging to $(5a'')^{-1}\ \tilde{X}\,^2A''$, $(4a'')^{-1}\ \tilde{A}\,^2A'$, $(21a')^{-1}\ \tilde{B}\,^2A'$ and $(20a')^{-1}\ \tilde{C}\,^2A'$ ionic states of 2(5H)-thiophenone. See text for details.

Fig. 1 The VUV photoabsorption cross-section in the 3.7–10.7 eV photon energy range for 2(5H)-thiophenone. Inset shows the structure of the molecule with atoms numbering.

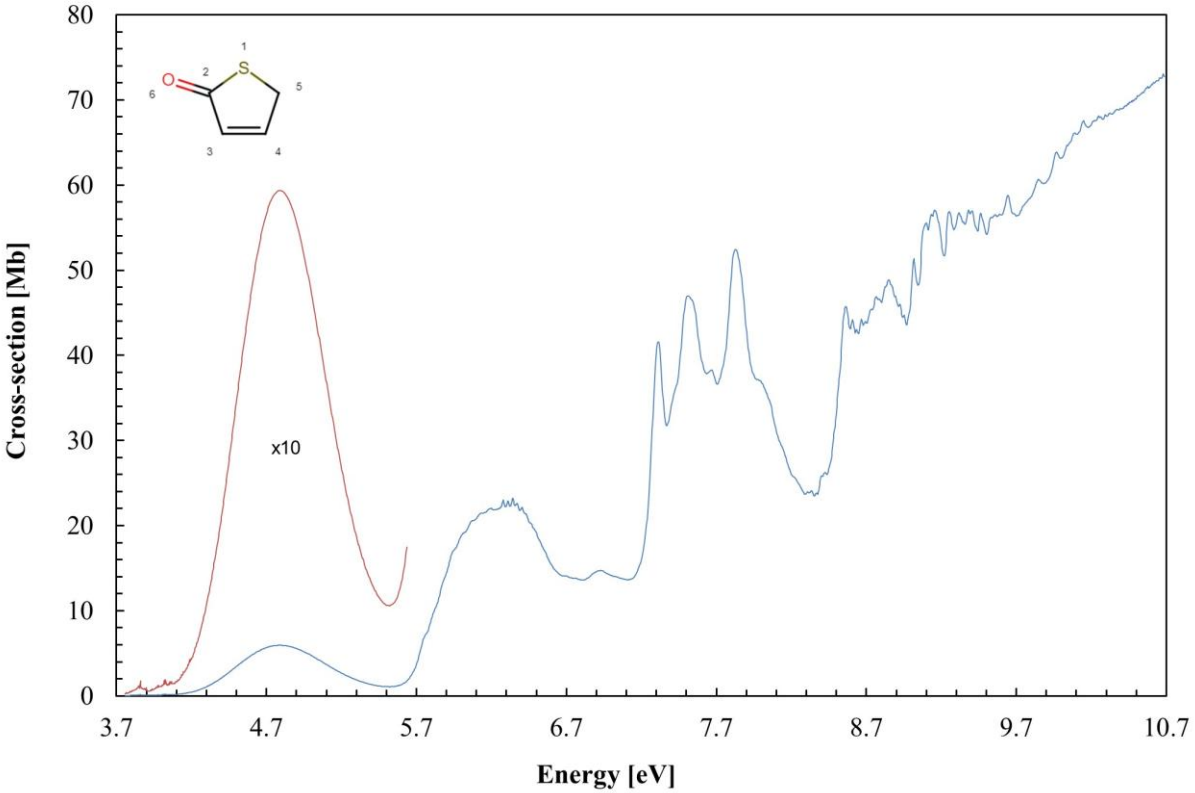

Fig. 2 The VUV photoabsorption cross-section of 2(5H)-thiophenone in the: (a) 3.7–6.0 eV and (b) 3.7–4.5 eV photon energy ranges.

(a)

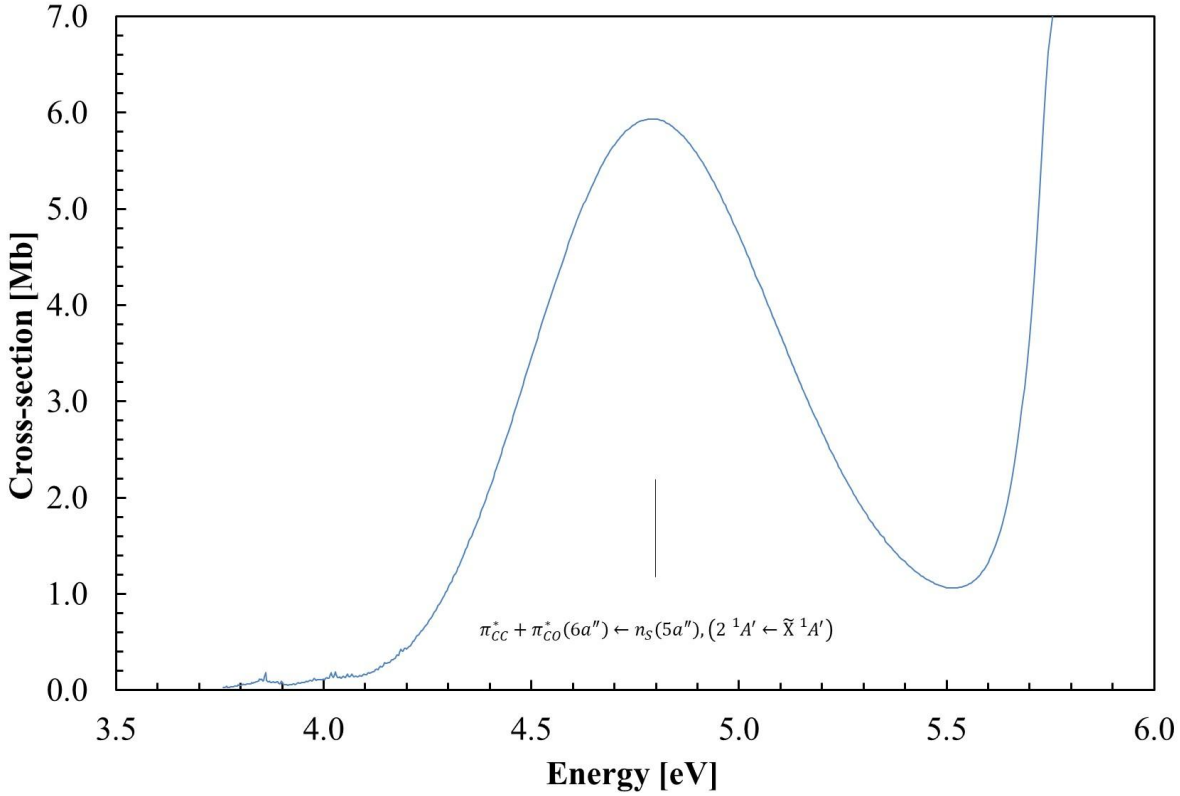

(b)

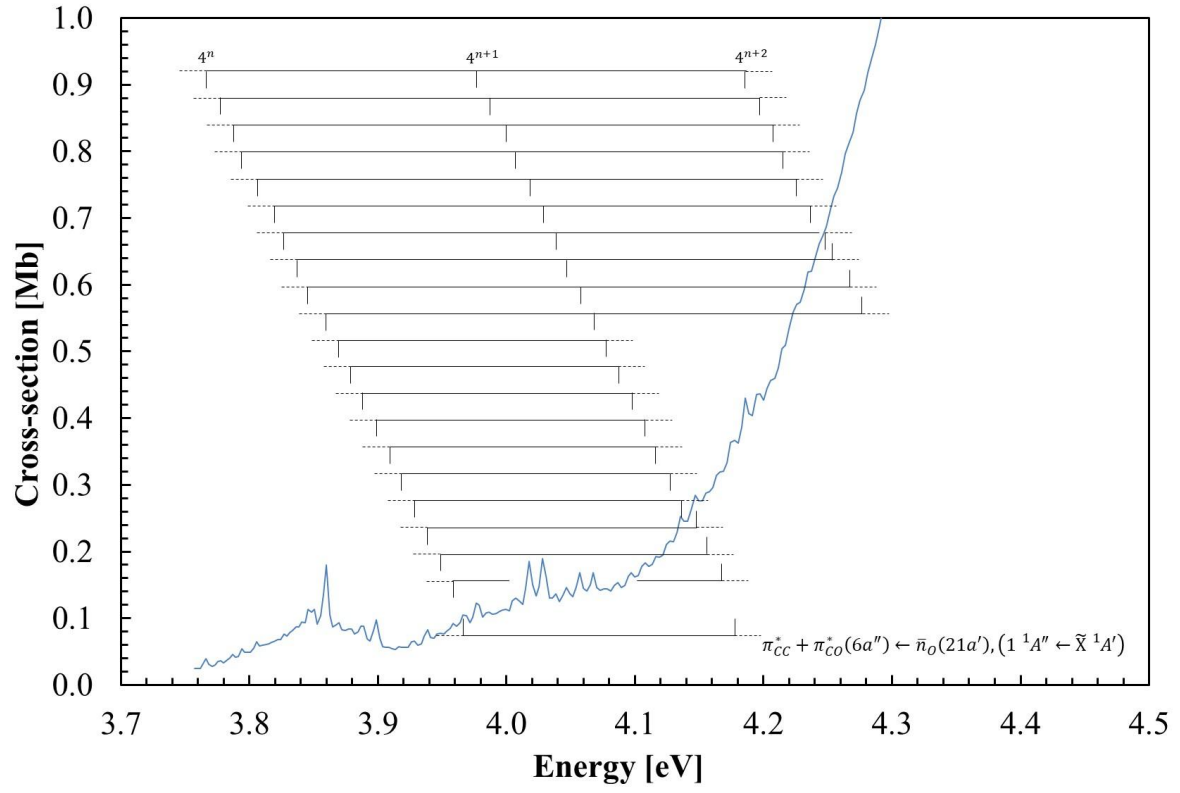

Fig. 3 The VUV photoabsorption cross-section in the 5.5–7.0 eV photon energy range for 2(5H)-thiophenone.

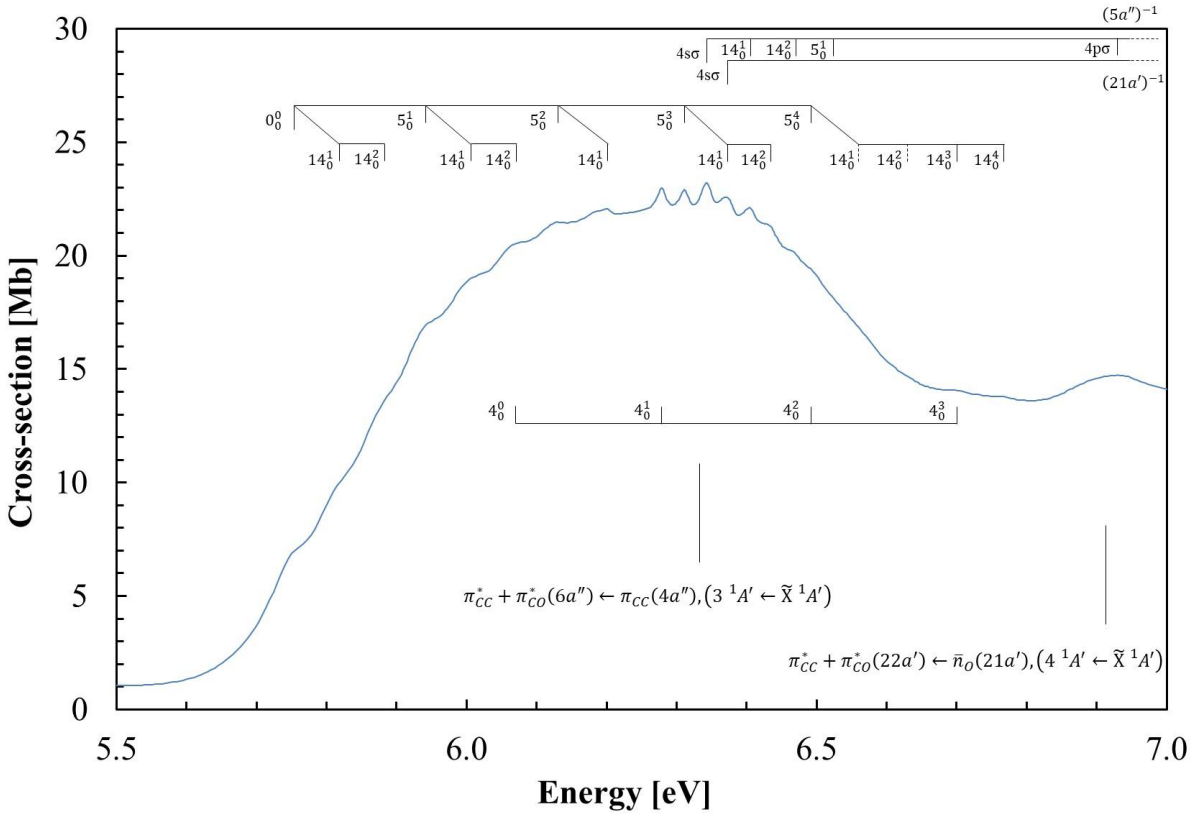

Fig. 4 The VUV photoabsorption cross-section in the 7.0–8.5 eV photon energy range for 2(5H)-thiophenone.

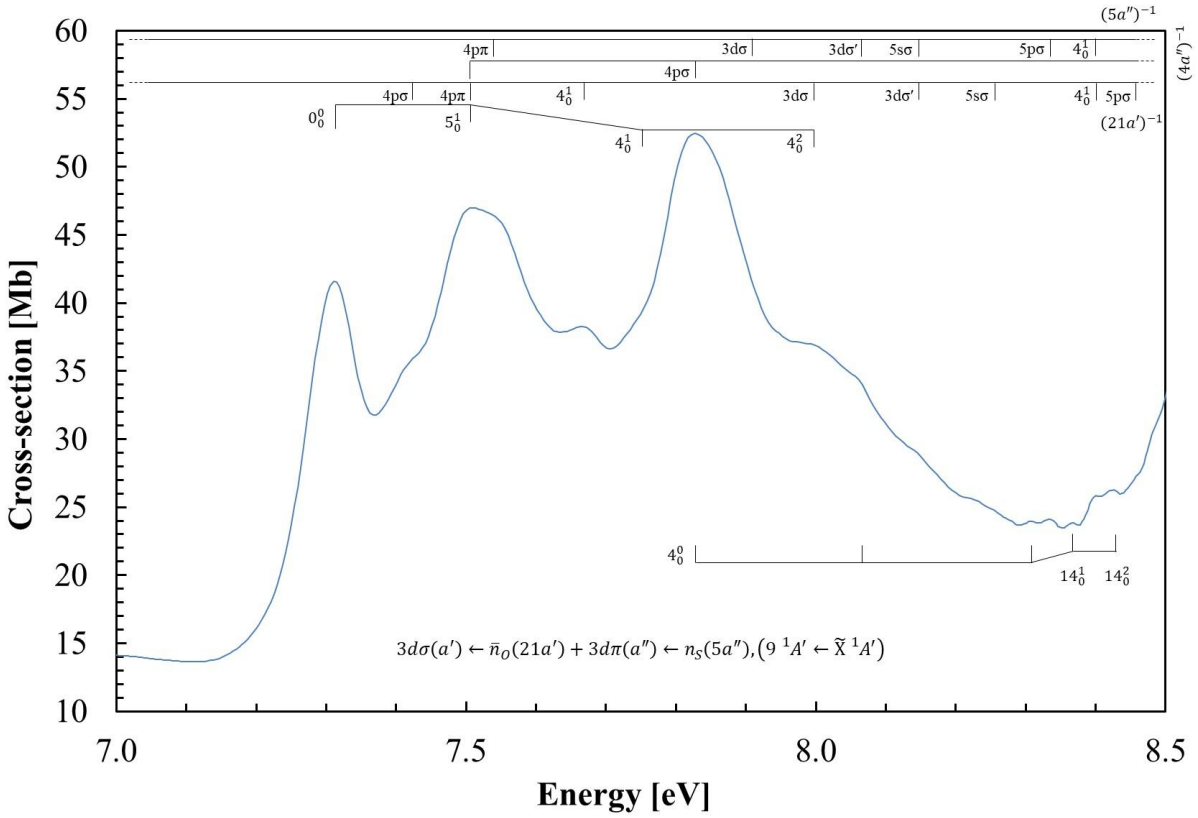

Fig. 5 The VUV photoabsorption cross-section in the 8.5–10.7 eV photon energy range for 2(5H)-thiophenone.

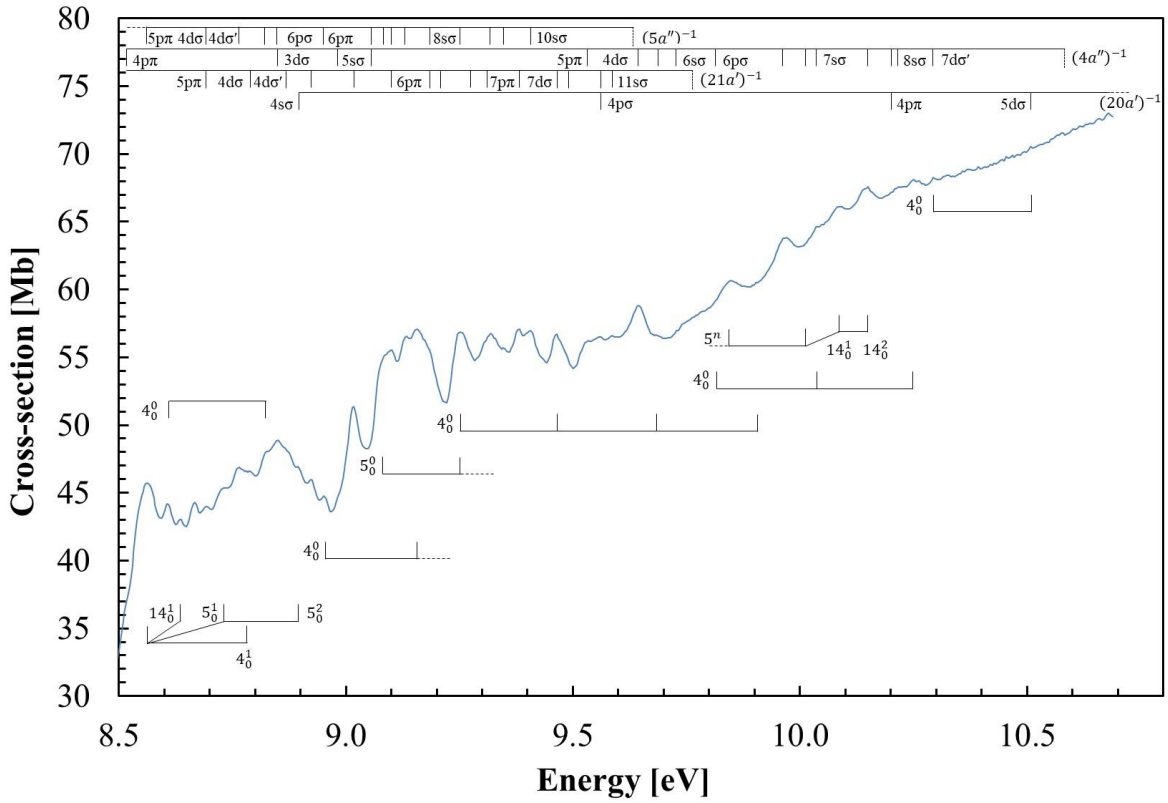

Table 1 Calculated vertical excitation energies (EOM-CCSD/aug-cc-pV(T+d)Z+R basis set) and oscillator strengths (singlet states) of 2(5H)-thiophenone (C_4H_4OS), compared with results from the present experimental data (all energies in eV). For a complete table see Supplementary Material Table S1. See details in text.

State	E (eV)	f_L	$\langle r^2 \rangle$ [a]	HOMO	HOMO-1	HOMO-2	Mixed Character	Exp. (eV) [b]	Cross-section (Mb)
				n_S (5a″)	π_{CC} (4a″)	n_O(21a′)			
$\tilde{X}$ ^{1}A′	–	–	95						
1 ^{1}A"	4.420	0.00039	94			$\pi^*_{CC} + \pi^*_{CO}$ (6a")		4.028	0.19
2 ^{1}A'	5.340	0.05785	96	$\pi^*_{CC} + \pi^*_{CO}$ (6a")				4.787	5.94
3 ^{1}A'	6.689	0.14547	99		$\pi^*_{CC} + \pi^*_{CO}$ (6a")			6.344	23.21
4 ^{1}A'	6.943	0.07573	110			$\pi^*_{CC} + \pi^*_{CO}$ (22a')		6.93(0)	14.73
4 ^{1}A"	7.193	0.01023	138	4pσ (a')				6.93(0)	14.73
6 ^{1}A'	7.260	0.01126	144	4pπ (a")				7.54(2)	46.15
7 ^{1}A'	7.592	0.04367	145			4pσ (a')		7.42(4)(s)	35.94
9 ^{1}A'	7.873	0.09247	144				n_S (5a") → 3dπ (a") + n_O (21a') → 3dσ (a')	7.827	52.46
10 ^{1}A'	8.056	0.07646	170			3dσ' (a')		7.99(9)(s)	42.68
18 ^{1}A'	8.742	0.03732	369			5pσ (a')		8.850	48.88
23 ^{1}A'	8.924	0.02137	346				π_{CC} (4a") → 3dπ (a") + n_S (5a") → 4dπ' (a")	9.160	57.07
28 ^{1}A"	8.965	0.01778	190		5sσ (a')			9.05(7)(s)	48.97

[a] Mean value of r^2 (electronic radial spatial extents)

[b] the last decimal on the energy value is given in brackets for these less-resolved features

Table 2 Proposed vibrational assignments of 2(5H)-thiophenone absorption band in the photon energy range 3.7−4.5 eV[a]. Energies in eV. See text for details.

assignment	energy	ΔE (υ_4')	ΔE (υ_5')	ΔE (υ_{14}')
$\pi^*_{CC} + \pi^*_{CO}(6a'') \leftarrow \bar{n}_O(21a'), \left(1\,^1A'' \leftarrow \tilde{X}\,^1A'\right)$				
4^n	3.766	–	–	–
4^n	3.77(5)(b)	–	–	–
4^n	3.787	–	–	–
4^n	3.794	–	–	–
4^n	3.806	–	–	–
4^n	3.82(2)(b)	–	–	–
4^n	3.827	–	–	–
$4^n + 14_0^1/4^n$	3.83(9)(s)	–	–	0.073
$4^n + 14_0^1/4^n$	3.846	–	–	0.071
$4^n + 14_0^1/4^n$	3.860	–	–	0.073
$4^n + 14_0^1/4^n$	3.870	–	–	0.076
$4^n + 14_0^1/4^n$	3.87(7)(b)	–	–	0.071
$4^n + 14_0^1/4^n$	3.88(9)(b)	–	–	0.077
$4^n + 14_0^1/4^n$	3.899	–	–	0.072
$4^n + 14_0^2/4^n + 14_0^1/4^n$	3.90(6)(b)	–	–	0.067
$4^n + 14_0^2/4^n + 14_0^1/4^n$	3.916	–	–	0.070
$4^n + 14_0^2/4^n + 14_0^1/4^n$	3.926	–	–	0.066
$4^n + 14_0^2/4^n + 14_0^1/4^n$	3.938	–	–	0.068
$4^n + 14_0^2/4^n + 14_0^1/4^n$	3.94(8)(s)	–	–	0.071
$4^n + 14_0^2/4^n + 14_0^1/4^n/4^n + 5_0^1$	3.95(8)(s)	–	0.192	0.069
$4^n + 14_0^2/4^n + 14_0^1/4^n/4^n + 5_0^1$	3.96(6)(b)	–	0.191	0.067
$4^{n+1}/4^n + 5_0^1$	3.976	0.210	0.189	–
$4^{n+1}/4^n + 14_0^1/4^n + 5_0^1$	3.984	0.209	0.190	0.068
$4^{n+1}/4^n + 14_0^1/4^n + 5_0^1$	4.00(0)(w)	0.213	0.194	0.074
$4^{n+1}/4^n + 14_0^1/4^n + 5_0^1$	4.007	0.213	0.185	0.069
$4^{n+1}/4^n + 14_0^1/4^n + 5_0^1$	4.018	0.212	0.191	0.070
$4^{n+1}/4^n + 14_0^1/4^n + 5_0^1$	4.028	0.206	0.189	0.080
$4^{n+1}/4^n + 14_0^1/4^n + 5_0^1$	4.039	0.212	0.193	0.081
$4^{n+1}/4^n + 5_0^1$	4.046	0.207	0.186	–
$4^{n+1}/4^{n+1} + 14_0^1/4^n + 14_0^2/4^n + 5_0^1$	4.057	0.211	0.187	0.073
$4^{n+1}/4^{n+1} + 14_0^1/4^n + 14_0^2/4^n + 5_0^1$	4.068	0.208	0.191	0.068
$4^{n+1}/4^{n+1} + 14_0^1/4^n + 14_0^2/4^n + 5_0^1$	4.07(8)(b)	0.208	0.189	0.071
$4^{n+1}/4^{n+1} + 14_0^1/4^n + 14_0^2$	4.086	0.209	–	0.068

$4^{n+1}/4^{n+1} + 14_0^1/4^n + 14_0^2$	4.097	0.208	−	0.069
$4^{n+1}/4^{n+1} + 14_0^1/4^n + 14_0^2$	4.108	0.209	−	0.069
4^{n+1}	4.116	0.210	−	−
$4^{n+1}/4^{n+1} + 14_0^1/4^{n+1} + 14_0^2/4^n + 14_0^3$	4.127	0.211	−	0.070
$4^{n+1}/4^{n+1} + 14_0^1/4^{n+1} + 14_0^2/4^n + 14_0^3$	4.136	0.210	−	0.068
$4^{n+1}/4^{n+1} + 14_0^1/4^{n+1} + 14_0^2/4^n + 14_0^3/4^n + 5_0^2$	4.147	0.209	0.189	0.069
$4^{n+1}/4^{n+1} + 14_0^1/4^{n+1} + 14_0^2/4^n + 14_0^3/4^n + 5_0^2$	4.15(8)(s)	0.210	0.192	0.072
$4^{n+1}/4^{n+1} + 14_0^1/4^{n+1} + 14_0^2/4^n + 14_0^3/4^n + 5_0^2$	4.16(9)(s)	0.211	0.193	0.072
$4^{n+1}/4^{n+1} + 14_0^1/4^{n+1} + 14_0^2/4^n + 14_0^3/4^n + 5_0^2$	4.177	0.211	0.193	0.069
$4^{n+2}/4^n + 5_0^2$	4.186	0.210	0.186	−
$4^{n+2}/4^n + 5_0^2$	4.19(4)(b)	0.210	0.187	−
$4^{n+2}/4^n + 14_0^4/4^n + 5_0^2$	4.20(6)(s)	0.206	0.188	0.079
$4^{n+2}/4^n + 14_0^4/4^n + 5_0^2$	4.21(4)(s)	0.207	0.186	0.078
$4^{n+2}/4^n + 14_0^4/4^n + 5_0^2$	4.22(6)(s)	0.208	0.187	0.079
$4^{n+2}/4^n + 14_0^4/4^n + 5_0^2$	4.23(7)(s)	0.209	0.191	0.079
$4^{n+2}/4^n + 14_0^4/4^n + 5_0^1$	4.24(9)(s)	0.210	0.192	0.080
$4^{n+2}/4^n + 5_0^1$	4.25(8)(s)	0.212	0.190	−
$4^{n+2}/4^n + 5_0^2$	4.26(7)(s)	0.210	0.189	−
$4^{n+2} + 14_0^1/4^n + 14_0^5$	4.27(5)(s)	0.207	−	0.069

[a] (b) broad structure; (s) shoulder structure; (w) weak feature (the last decimal of the energy value is given in brackets for these less-resolved features);

Table 3 Proposed vibrational assignments of 2(5H)-thiophenone absorption bands in the photon energy range 5.5–8.5 eV[a]. Energies in eV. See text for details.

assignment	energy	ΔE (υ_4')	ΔE (υ_5')	ΔE (υ_{14}')
$\pi^*_{CC} + \pi^*_{CO}(6a'') \leftarrow \pi_{CC}(4a''), \left(3\,^1A' \leftarrow \tilde{X}\,^1A'\right)$				
0_0^0	5.75(6)(s)	–	–	–
14_0^1	5.82(1)(s)	–	–	0.065
14_0^2	5.88(7)(s)	–	–	0.066
5_0^1	5.94(7)(s)	–	0.191	–
$5_0^1 + 14_0^1$	6.01(0)(s)	–	–	0.063
$5_0^1 + 14_0^2$	6.07(5)(s)	–	–	0.065
5_0^2	6.13(5)(s)	–	0.188	–
$5_0^2 + 14_0^1$	6.20(2)(b)	–	–	0.067
$5_0^1 + 14_0^2 + 4_0^1$	6.281	0.206	–	–
5_0^3	6.311	–	0.176	–
$4s\sigma(5a'')^{-1}$	6.344	–	–	–
$5_0^3 + 14_0^1 / 4s\sigma(21a')^{-1}$	6.37(1)(b)	–	–	0.060
$4s\sigma(5a'')^{-1} + 14_0^1$	6.406	–	–	0.062
$5_0^3 + 14_0^2 / 4s\sigma(21a')^{-1} + 14_0^1$	6.43(4)(s)	–	–	0.063
$4s\sigma(5a'')^{-1} + 14_0^2$	6.46(8)(s)	–	–	0.062
$5_0^4 / 4_0^2$	6.49(5)(s)	0.214	0.184	–
$4s\sigma(5a'')^{-1} + 5_0^1$	6.52(2)(s)	–	0.178	–
$5_0^4 + 14_0^1$	6.55(7)(s,w)	–	–	0.062
$5_0^4 + 14_0^2$	6.63(0)(s,w)	–	–	0.073
$5_0^4 + 14_0^3 / 4_0^3$	6.70(2)(b,w)	0.207	–	0.072
$5_0^4 + 14_0^4$	6.76(8)(b,w)	–	–	0.066
$3d\sigma(a') \leftarrow \bar{n}_O(21a') + 3d\pi(a'') \leftarrow n_S(5a''), \left(9\,^1A' \leftarrow \tilde{X}\,^1A'\right)$				
0_0^0	7.315	–	–	–
$4p\sigma(21a')^{-1}$	7.42(4)(s)	–	–	–
$5_0^1 / 4p\pi(21a')^{-1}$	7.51(0)(b)	–	0.195	–
$4p\sigma(21a')^{-1} + 4_0^1$	7.66(8)(b)	0.244	–	–
$5_0^1 + 4_0^1 / 4p\pi(21a')^{-1} + 4_0^1$	7.75(4)(s)	0.244	–	–

$4p\sigma(4a'')^{-1}$	7.827	–	–	–
$5_0^1 + 4_0^2/4p\pi(21a')^{-1} + 4_0^2/3d\sigma(21a')^{-1}$	7.99(9)(s)	0.245	–	–
$5s\sigma(5a'')^{-1}/3d\sigma'(21a')^{-1}$	8.14(6)(s)	–	–	–
$4p\sigma(4a'')^{-1} + 4_0^1/3d\sigma'$	8.06(7)(s)	0.240	–	–
$4p\sigma(4a'')^{-1} + 4_0^2/3d\sigma' + 4_0^1$	8.30(4)(b)	0.237	–	–
$4p\sigma(4a'')^{-1} + 4_0^2 + 14_0^1/3d\sigma' + 4_0^1 + 14_0^1$	8.366	–	–	0.062
$5s\sigma(5a'')^{-1} + 4_0^1/3d\sigma'(21a')^{-1} + 4_0^1$	8.39(7)(s)	0.251	–	–
$4p\sigma(4a'')^{-1} + 4_0^2 + 14_0^2/3d\sigma' + 4_0^1 + 14_0^2$	8.42(6)(b)	–	–	0.060

[a] (s) shoulder structure; (b) broad structure; (w) weak feature (the last decimal of the energy value is given in brackets for these less-resolved features);

Table 4 Proposed vibrational assignments of 2(5H)-thiophenone absorption bands in the photon energy range 8.2−10.7 eV[a]. Energies in eV. See text for details.

assignment	energy	ΔE (υ_4')	ΔE (υ_5')	ΔE (υ_{14}')
$5s\sigma(21a')^{-1}$	8.25(5)(s,w)	–	–	–
$5s\sigma(21a')^{-1} + 4_0^1$	8.48(3)(s)	0.228	–	–
$5p\pi(5a'')^{-1}$	8.562	–	–	–
4_0^0	8.607	–	–	–
$5p\pi(5a'')^{-1} + 14_0^1$	8.637	–	–	0.075
$5s\sigma(21a')^{-1} + 4_0^1 + 5_0^1$	8.667	–	0.184	–
$5p\pi(5a'')^{-1} + 5_0^1$	8.73(7)(s)	–	0.175	–
$5p\pi(5a'')^{-1} + 4_0^1/4d\sigma(21a')^{-1}$	8.78(7)(s)	0.225	–	–
$4_0^1/6s\sigma(5a'')^{-1}$	8.82(8)(s)	0.221	–	–
$5s\sigma(21a')^{-1} + 4_0^1 + 5_0^2/4d\sigma'(21a')^{-1}$	8.86(3)(s)	–	0.196	–
$5p\pi(5a'')^{-1} + 5_0^2/4s\sigma(20a')^{-1}$	8.891	–	0.154	–
$6p\pi(5a'')^{-1}$	8.952	–	–	–
$5d\sigma'(5a'')^{-1}$	9.08(6)(s)	–	–	–
$6p\pi(5a'')^{-1} + 4_0^1$	9.157	0.205	–	–
$5d\sigma'(5a'')^{-1} + 5_0^1/8s\sigma(5a'')^{-1}/6d\sigma'(5a'')^{-1}/5p\sigma(5a'')^{-1}$	9.253	–	0.167	–
$8s\sigma(5a'')^{-1} + 4_0^1/6d\sigma'(5a'')^{-1} + 4_0^1/5p\sigma(5a'')^{-1} + 4_0^1/7d\sigma(21a')^{-1} + 4_0^1$	9.461	0.208	–	–
$8s\sigma(5a'')^{-1} + 4_0^2/6d\sigma'(5a'')^{-1} + 4_0^2/5p\sigma(5a'')^{-1} + 4_0^2/4d\sigma'(4a'')^{-1} + 4_0^2$	9.69(0)(s)	0.229	–	–

$6p\sigma(4a'')^{-1}$	9.81(7)(s,w)	–	–	–
$8s\sigma(5a'')^{-1} + 4_0^3/6d\sigma'(5a'')^{-1} + 4_0^3/5p\sigma(5a'')^{-1} + 4_0^3$	9.90(3)(s,w)	0.213	–	–
5^n	9.844	–	–	–
$5^{n+1}/5d\sigma'(4a'')^{-1}$	10.01(5)(s,w)	–	0.171	–
$6p\sigma(4a'')^{-1} + 4_0^1/7s\sigma(4a'')^{-1}$	10.03(5)(w)	0.218	–	–
$5^{n+1} + 14_0^1/5d\sigma'(4a'')^{-1} + 14_0^1$	10.08(4)(b)	–	–	0.069
$5^{n+1} + 14_0^2/5d\sigma'(4a'')^{-1} + 14_0^2/6d\sigma(4a'')^{-1}$	10.150	–	–	–
$6p\sigma(4a'')^{-1} + 4_0^2/7s\sigma(4a'')^{-1} + 4_0^1$	10.251	0.216	–	–
$7d\sigma'(4a'')^{-1}$	10.293	–	–	–
$5d\sigma(20a')^{-1} + 4_0^1$	10.50(7)(w)	0.214	–	–

[a] (s) shoulder structure; (w) weak feature; (b) broad structure (the last decimal of the energy value is given in brackets for these less-resolved features);

Table 5 Energy values (eV), quantum defects (δ) and assignments of the Rydberg series converging to $(5a'')^{-1}$ $\tilde{X}\,^2A''$, $(4a'')^{-1}$ $\tilde{A}\,^2A''$, $(21a')^{-1}$ $\tilde{B}\,^2A'$ and $(20a')^{-1}$ $\tilde{C}\,^2A'$ ionic states of 2(5H)-thiophenone. See text for details.

E_n	δ	Assignment	E_n	δ	Assignment	E_n	δ	Assignment	E_n	δ	Assignment
$(IE_1)_v$ = 9.63 eV $(5a'')^{-1}$			**$(IE_2)_{ad}$ = 10.58 eV $(4a'')^{-1}$**			**$(IE_3)_{ad}$ = 9.76 eV $(21a')^{-1}$**			**$(IE_4)_v$ = 12.25 eV $(20a')^{-1}$**		
(nsσ ← 5a″)			*(nsσ ← 4a″)*			*(nsσ ← 21a′)*			*(nsσ ← 20a′)*		
6.344	1.96	4sσ	7.51(0)(b)	1.89	4sσ	6.37(1)(b)	2.00	4sσ	8.891	1.99	4sσ
8.14(6)(s)	1.97	5sσ	9.05(7)(s)	2.01	5sσ	8.25(5)(s,w)	1.99	5sσ	*(npσ ← 20a′)*		
8.82(8)(s)	1.88	6sσ	9.72(8)(w)	2.00	6sσ	8.923	1.97	6sσ	9.54(8)(b,w)	1.76	4pσ
9.100	1.93	7sσ	10.03(5)(w)	2.00	7sσ	9.20(8)(s)	2.03	7sσ	*(npπ ← 20a′)*		
9.253	1.99	8sσ	10.21(7)(w)	1.88	8sσ	9.382	2.00	8sσ	10.19(6)(s,w)	1.43	4pπ
9.350	2.03	9sσ	*(npσ ← 4a″)*			9.48(6)(s)	1.95	9sσ	*(ndσ ← 20a′)*		
9.407	2.19	10sσ	7.827	1.78	4pσ	9.54(8)(b,w)	1.99	10sσ	10.50(7)(w)	0.21	3dσ
(npσ ← 5a″)			9.253	1.80	5pσ	9.585	2.18	11sσ			
6.93(0)(b)	1.75	4pσ	9.81(7)(s,w)	1.78	6pσ	*(npσ ← 21a′)*					
8.33(5)(b)	1.76	5pσ	*(npπ ← 4a″)*			7.42(4)(s)	1.59	4pσ			
8.847	1.83	6pσ	8.51(8)(s)	1.43	4pπ	8.46(3)(s)	1.76	5pσ			
9.137	1.75	7pσ	9.537	1.39	5pπ	9.017	1.72	6pσ			
(npπ ← 5a″)			9.96(3)(b)	1.30	6pπ	9.27(0)(s)	1.73	7pσ			
7.54(2)(s,w)	1.45	4pπ	*(ndσ ← 4a″)*			*(npπ ← 21a′)*					
8.562	1.43	5pπ	8.847	0.20	3dσ	7.51(0)(b)	1.54	4pπ			

8.952	1.52	6pπ	9.645	0.18	4dσ	8.698	1.42	5pπ	
9.18(4)(s)	1.48	7pπ	9.96(3)(b)	0.30	5dσ	9.100	1.46	6pπ	
9.319	1.39	8pπ	10.150	0.37	6dσ	9.31(2)(s)	1.49	7pπ	
(ndσ ← 5a″)			*(ndσ′ ← 4a″)*			*(ndσ ← 21a′)*			
7.90(2)(s,w)	0.19	3dσ	8.98(4)(s)	0.08	3dσ′	7.99(9)(s)	0.22	3dσ	
8.698	0.18	4dσ	9.69(0)(s)	0.09	4dσ′	8.78(7)(s)	0.26	4dσ	
9.05(7)(s)	0.13	5dσ	10.01(5)(s,w)	0.09	5dσ′	9.154	0.26	5dσ	
(ndσ′ ← 5a″)			10.19(6)(s,w)	0.05	6dσ′	–	–	–	
8.06(7)(s)	0.05	3dσ′	10.293	0.11	7dσ′	9.461	0.25	7dσ	
8.765	0.03	4dσ′				*(ndσ ← 21a′)*			
9.08(6)(s)	0.00	5dσ′				8.14(6)(s)	0.10	3dσ′	
9.253	0.00	6dσ′				8.86(3)(s)	0.10	4dσ′	
9.350	0.03	7dσ′				9.18(4)(s)	0.14	5dσ′	

(s) shoulder structure; (b) broad feature; (w) weak structure (the last decimal on the energy value is given in brackets for these less-resolved features).

TOC Graphic